Journal of Sound and Vibration (1998) **217**(4), 737–756
Article No. sv981804

IDENTIFICATION OF NON-LINEAR HYSTERETIC ISOLATORS FROM PERIODIC VIBRATION TESTS

Y. Q. Ni, J. M. Ko and C. W. Wong

Department of Civil and Structural Engineering,
The Hong Kong Polytechnic University, *Kowloon*, *Hong Kong*

(*Received* 28 *July* 1997, *and in final form* 28 *May* 1998)

This paper addresses the parameter identification of friction-type hysteretic isolators based on the versatile Bouc–Wen differential model. A frequency domain method is developed to identify the model parameters from the experimental data of periodic vibration tests. All the five parameters in the hysteretic model are obtained by a one-stage parameter estimate scheme. Numerical simulations show that the proposed method is insensitive to the noise in the observation signals. This method is then implemented to model and identify the experimental hysteresis loops of wire–cable vibration isolators, and the accuracy of the parameter identification is verified by comparing the measured and identified harmonic components of the hysteretic restoring force.

1. INTRODUCTION

The non-linear hysteretic isolators with friction damping performance have application in many areas [1–5]. They are capable of both attenuating heavy shock and absorbing broad band vibration. Of particular importance for vibration control at resonance is their slippage and flexure hysteresis. The non-linear restoring force of hysteretic isolators is history-dependent, i.e., it depends not only on the instantaneous deformation but also on the past history of deformation. As a result, the hysteretic restoring force cannot be expressed by an algebraic function of the instantaneous displacement and velocity. This memory nature renders the hysteretic systems more difficult to model and analyze than other non-linear systems.

The Bouc–Wen model [6, 7] has been widely used to describe non-linear hysteretic systems including hysteretic isolators [8–11]. This non-linear differential equation model reflects local history dependence through introducing an extra state variable. Through appropriate choices of parameters in the model, it can represent a wide variety of softening or hardening, smoothly varying or nearly bilinear hysteretic behavior. This model has also been generalized to include hysteresis pinching and stiffness/strength degradation. As a versatile model, it is often possible to obtain a satisfactory representation of actual, measured hysteresis loops when the model parameters are properly selected. Once one set of

0022–460X/98/440737 + 20 $30.00/0

parameters are determined by identification from experimental data, this model can automatically describe all hysteresis loops with different excitation/response amplitudes from the experimental values.

In the past decade, efforts have been devoted to developing the identification procedures for non-linear hysteretic systems. Most of them were presented by referring to the Bouc–Wen model due to its significant advantage. These procedures include the time-domain least-squares method [12, 13], the time domain extended Kalman filtering technique [14, 15], and sequential or adaptive method [16, 17]. A frequency domain Kalman filtering algorithm using response statistics has also been proposed for the identification of hysteretic systems under random excitation [18]. Two kinds of treatment were alternatively adopted in these identification procedures. For the first kind of treatment, the exponential parameter in the Bouc–Wen model is taken as a known constant and only other model parameters need to be identified [13–15, 17, 18]. Such treatment may result in a linear estimate scheme or avoid the divergency of non-linear iterative algorithms. However, *a priori* assumption of the exponential parameter will certainly reduce, more or less, the identification accuracy. The second kind of treatment is the introduction of a two-stage estimate scheme [12, 16]. In the first stage, one or two parameters are fixed to the assumed values and the remaining parameters are estimated. The second stage takes the final estimate of the first stage as an initial estimate and carries out the identification referring to all the model parameters. Recently, a three-stage estimate scheme was proposed [19] wherein different estimate techniques are used in the three stages. The multi-stage estimate approach is usually time consuming although it can ameliorate identification accuracy as well as convergency.

Wire–cable (rope) isolators are typical non-linear hysteretic damping devices. They adopt stranded wire rope as the elastic component and utilize inherent friction damping between the strands of the wire rope. Wire–cable isolators have found numerous applications in the shock and vibration isolation of industrial and defense equipment, electronic systems, critical machinery and other sensitive equipment [1, 20, 21]. Recently, the usefulness of these isolators for the seismic protection of equipment in buildings was investigated [11]. The potentially greater use of wire–cable isolators requires a full understanding of their damping characteristics. Only little theoretical work has been done on the analytical modelling of wire–cable isolators. Cutchins *et al*. [1] proposed two Coulomb damper models in an effort to model the hysteretic damping of a wire rope isolation system. Subsequently, an amended model incorporating nth power velocity damping and non-linear stiffness was suggested to get a better match with experimental data [21]. With this model, the experimental hysteresis loops with different amplitudes cannot be represented by using a same set of model parameters. This model may also give an unreasonable indication of dynamic characteristics in some situations [22]. Ko *et al*. [23] proposed a semi-empirical model for representing a set of experimental hysteresis loops of a wire-cable isolator. Lo *et al*. [9] were among the first to model wire–cable isolators using the Bouc–Wen model. Demetriades *et al*. [11] adopted an amended Bouc–Wen model

to obtain analytical descriptions for the experimental hysteresis loops of wire–cable isolators.

The intent of this paper is to develop a frequency domain parametric idenification method for the modelling of non-linear hysteretic isolators from periodic vibration experimental data. The periodic vibration tests on non-linear hysteretic isolators are usually feasible in laboratory. The Bouc–Wen model is adopted to represent the hysteretic damping characteristics, and all the five parameters in the model are determined by identification from a one-stage estimate scheme. The proposed method is then applied to the modelling of wire–cable isolators from experimental data.

2. HYSTERETIC MODEL

2.1. BOUC–WEN HYSTERETIC MODEL

By using the Bouc–Wen model, the restoring force–displacement relation of a hysteretic isolator can be expressed in terms of the following non-linear differential equation [7]

$$r(t) = \mu K x(t) + (1-\mu)K\bar{z}(t), \qquad \dot{\bar{z}}(t) = \bar{\alpha}\dot{x}(t) - \bar{\beta}|\dot{x}(t)|\bar{z}(t)|\bar{z}(t)|^{n-1} - \bar{\gamma}\dot{x}(t)|\bar{z}(t)|^{n}. \tag{1a, b}$$

A detailed explanation of the physical meaning of the model parameters is available [24]. By means of the transformation

$$z = (1-\mu)K\bar{z}, \qquad b = \mu K, \qquad \alpha = \bar{\alpha}(1-\mu)K,$$
$$\beta = \bar{\beta}[(1-\mu)K]^{1-n}, \qquad \gamma = \bar{\gamma}[(1-\mu)K]^{1-n}, \tag{2}$$

equation (1) can be rewritten as

$$r(t) = bx(t) + z(t), \qquad \dot{z}(t) = \alpha\dot{x}(t) - \beta|\dot{x}(t)|z(t)|z(t)|^{n-1} - \gamma\dot{x}(t)|z(t)|^{n} \tag{3a, b}$$

where $r(t)$ and $x(t)$ represent the restoring force and displacement. $z(t)$ is a hysteretic auxiliary variable. The overdot denotes the differentiation with respect to time t. b, α, β, γ and n are model parameters to be determined. Through the transformation, the number of model parameters is reduced from six in equation (1) to five in equation (3).

2.2. SUITABILITY AND LIMITATION

The response behavior of the Bouc–Wen hysteretic oscillator was investigated by the present authors [25]. Recently, the hysteresis loop characteristics of the Bouc–Wen model were further studied [26]. Based on this work, some conclusions concerning the suitability and limitation of the Bouc–Wen model to the representation of actual, observed hysteresis loops are summarized as follows. (a) Although $z(t)$ versus $x(t)$ already represents a hysteretic constitutive relation, the linear term $bx(t)$ in equation (3a) is necessary for expressing actual hysteresis loops of isolators. If excluding the linear term $bx(t)$, it follows that $r(t) = z(t)$ and

$$\partial r/\partial x = \alpha - [\gamma + \beta \operatorname{sgn}(\dot{x}) \operatorname{sgn}(r)]|r|^{n} \tag{4}$$

In this instance, $\partial r/\partial x$ varies only with r except relating to the sign of $\dot{x}$, regardless of x. When $r = 0$, $\partial r/\partial x$ is also equal to the constant α. This means that the hysteresis loops corresponding to different excitation and response levels would have the same slope at those points with same values of r and identical sgn $(\dot{x})$, which conflicts with the observed hysteresis loops of the actual isolators [9, 23]. This inconsistency can be obviated through including a non-hysteretic linear term $bx(t)$ (even non-linear term if needed) in the restoring force expression. When the linear term is considered, one has

$$\partial r/\partial x = b + \partial z/\partial x|_{z=r-bx} = b + \alpha - [\gamma + \beta \text{ sgn } (\dot{x}) \text{ sgn } (r - bx)]|r - bx|^n, \quad (5)$$

which is a function of both r and x.

(b) The Bouc–Wen model is rate-independent. In mathematics, *hysteresis* is directly defined as *a rate independent memory effect* [27]. In reality, memory effects may not be purely rate-independent as hysteresis is coupled with the viscosity-type memory. However, the hysteresis effect is usually dominant when the time evolution is not too fast. The rate-independent feature of hysteresis is consistent with the experimental findings of the friction-type hysteretic damping devices. Dynamic tests showed that the hysteresis loops of wire–cable isolators are almost independent of vibration frequency in the tested frequency range [11, 23].

(c) The Bouc–Wen model is capable of representing normal softening, hardening or quasi-linear hysteresis loops, but fails to describe more complicated hysteresis behaviors. Some isolators may exhibit unsymmetric hysteresis loops under symmetric excitation. The Bouc–Wen model cannot represent such unsymmetric hysteresis. This model is also incapable of describing the so-called soft–hardening hysteresis loops and the hardening hysteresis loops with overlapping loading envelope. Some modification to the Bouc–Wen model has been made to accommodate the actual, complicated hysteresis behaviors [26].

(d) In some special cases, different combinations of some parameters in the Bouc–Wen model may produce almost identical hysteresis loops. When the Bouc–Wen model is used to represent softening hysteresis loops, the extreme value of the hysteretic auxiliary variable $z(t)$ can be obtained as

$$z_m = [\alpha/(\beta + \gamma)]^{1/n}. \quad (6)$$

With the value of z_m unvaried, different combinations of the parameters β and γ can give rise to similar hysteresis loops. Figure 1 illustrates two groups of hysteresis loops, one with $\beta = \gamma = 0{\cdot}5$ and the other with $\beta = 0{\cdot}8$ and $\gamma = 0{\cdot}2$. They are almost identical. This is also the reason why the identification results of some simulation examples are distinct from the true values [15, 19]. However, these deviated estimate values of the model parameters still produce almost the same hysteresis loops as the true hysteresis loops. In this sense, these estimate values are still reasonable identification results. This is especially true for the identification of actual isolators because one just needs an accurate modelling of experimental hysteresis loops. One can also deal with this nearly redundant parameter pheonomenon in identification process. For instance, the estimate can be carried out by imposing the constraint $\beta > \gamma$, $\beta = \gamma$ and $\beta < \gamma$ respectively. When the system is *a priori* known to display softening hysteresis loops, an altered version

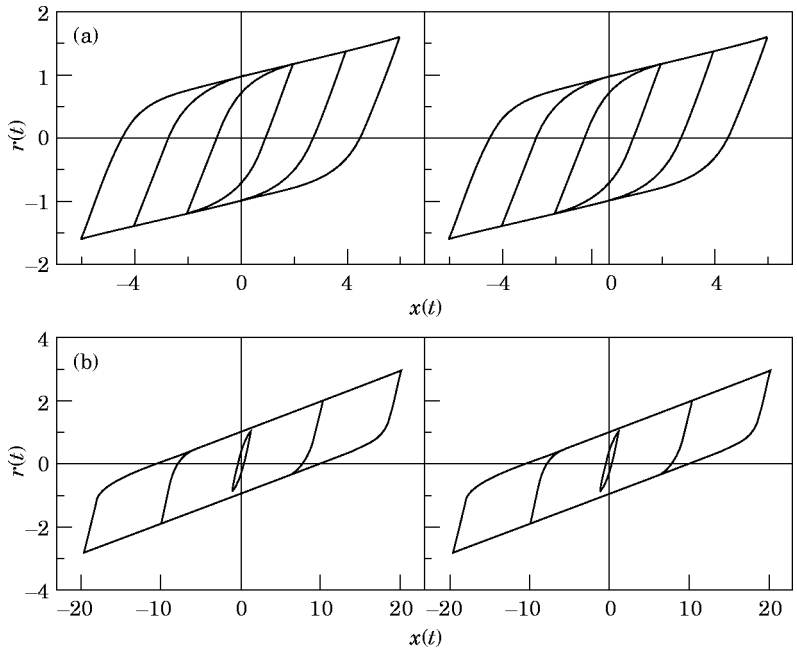

Figure 1. Comparison of hysteresis loops with different combinations of β and γ: (a) displacement controlled hysteresis loops ($b = 0{\cdot}1, \alpha = 1{\cdot}0, n = 1{\cdot}5$); (b) force controlled hysteresis loops ($b = 0{\cdot}1, \alpha = 1{\cdot}0, n = 1{\cdot}5$). Left figures $\beta = \gamma = 0{\cdot}5$; right figures $\beta = 0{\cdot}8$, $\gamma = 0{\cdot}2$.

of the Bouc–Wen model omitting the parameter γ may be adopted for identification. With the parameter γ omitted, the Bouc–Wen model reduces to Ozdemir's model [28]. The latter has also been used to model non-linear damping devices with softening hysteretic behavior [29, 30].

3. IDENTIFICATION METHOD

3.1. FREQUENCY DOMAIN ESTIMATE

Consider a hysteretic system for which the equation of motion is expressed as

$$m\ddot{x}(t) + r(t) = F(t), \tag{7}$$

where $x(t)$ represents the displacement response of a SDOF system or the generalized modal displacement of a MDOF system [31]. $F(t)$ and $r(t)$ are the (generalized modal) external excitation and hysteretic restoring force respectively. The mass m is assumed to be known. The hysteretic restoring force governed by equation (3) is identified by taking measurements of both the external excitation $F(t)$ and the displacement response $x(t)$ (or the acceleration $\ddot{x}(t)$ alternatively). The vector of model parameters to be identified is $\{\mathbf{y}\} = \{b\ \alpha\ \beta\ \gamma\ n\}^{\mathrm{T}}$.

For periodic vibration tests, the measured time signals of $F(t)$ and $x(t)$ are periodic and can be expressed as

$$F(t) = \frac{F_o}{2} + \sum_{j=1}^{N} F_j \cos \mathrm{j}\omega t + \sum_{j=1}^{N} F_j^* \sin \mathrm{j}\omega t,$$

$$x(t) = \frac{a_o}{2} + \sum_{j=1}^{N} a_j \cos \mathrm{j}\omega t + \sum_{j=1}^{N} a_j^* \sin \mathrm{j}\omega t, \tag{8, 9}$$

where

$$\{\mathbf{F}\} = \{F_0 \;\; F_1 \;\; F_2 \cdots F_N \;\; F_1^* \;\; F_2^* \cdots F_N^*\}^{\mathrm{T}}$$

and

$$\{\mathbf{a}\} = \{a_0 \;\; a_1 \;\; a_2 \cdots a_N \;\; a_1^* \;\; a_2^* \cdots a_N^*\}^{\mathrm{T}}$$

are the harmonic component vectors of $F(t)$ and $x(t)$ and ω is the vibration frequency. N is the order number of harmonics truncated. Usually, the excitation and response signals are recorded as digital data sampled at discrete time intervals. When the digital acquisition satisfies some specific conditions [23], the undistorted values of harmonic components of a periodic signal can be readily obtained by fast Fourier transform (FFT) to the sampled data. A numerical re-sampling process [26] can be used before FFT to insure that the sampled data completely meet such conditions. The model parameters $\{\mathbf{y}\}$ are now identified according to the known harmonic component vectors $\{\mathbf{F}\}$, $\{\mathbf{a}\}$ of the measured excitation and response periodic signals.

Introducing equation (3) into equation (7) yields

$$\dot{F} - m\dddot{x} = \dot{x}\{b + \alpha - [\beta \operatorname{sgn}(\dot{x}) \operatorname{sgn}(F - bx - m\ddot{x}) + \gamma]|F - bx - m\ddot{x}|^n\}. \tag{10}$$

The time domain determining function is therefore defined as

$$D(t) = \dot{F} - m\dddot{x} - \dot{x}\{b + \alpha - [\beta \operatorname{sgn}(\dot{x}) \operatorname{sgn}(F - bx - m\ddot{x}) + \gamma]|F - bx - m\ddot{x}|^n\}. \tag{11}$$

If the actual force–displacement relation conforms completely to the Bouc–Wen model and $\{\mathbf{y}\}$ is true model parameters, applying the Galerkin (harmonic balance) method into equation (11) achieves

$$\mathbf{d}(\mathbf{y}) = \mathbf{0}, \tag{12}$$

where $\{\mathbf{d}\} = \{\mathbf{d}(\mathbf{y})\} = \{d_0 \;\; d_1 \;\; d_2 \cdots d_N \;\; d_1^* \;\; d_2^* \cdots d_N^*\}^{\mathrm{T}}$ is the harmonic component vector of $D(t)$ corresponding to the model parameters $\{\mathbf{y}\}$. For the identification problem, the determining function is usually impossible to approach zero due to model error and measurement noise. In this situation, $\{\mathbf{d}\}$ is interpreted as the residual of the equations and a minimization problem in terms of non-linear least squares arises as

$$\min g(\mathbf{y}) = \|\mathbf{d}(\mathbf{y})\|^2 = \mathbf{d}^{\mathrm{T}}\mathbf{d}. \tag{13}$$

This non-linear least squares optimal problem is solved iteratively by the Levenberg–Marquardt (LM) algorithm. The iteration formula of the LM algorithm is

$$\mathbf{y}^{(k+1)} = \mathbf{y}^{(k)} - \{\mathbf{J}[\mathbf{y}^{(k)}]^{\mathrm{T}} \cdot \mathbf{J}[\mathbf{y}^{(k)}] + \varphi_k \mathbf{I}\}^{-1} \cdot \mathbf{J}[\mathbf{y}^{(k)}]^{\mathrm{T}} \cdot \mathbf{d}[\mathbf{y}^{(k)}], \tag{14}$$

where $\mathbf{J}[\mathbf{y}^{(k)}] = \partial \mathbf{d}(\mathbf{y})/\partial \mathbf{y}|\mathbf{y} = \mathbf{y}^{(k)}$ is the Jacobian matrix, φ_k is the Levenberg–Marquardt parameter, $\mathbf{I}$ is the identity matrix.

At each iteration step, the function vector $\mathbf{d}[\mathbf{y}^{(k)}]$ and Jacobian matrix $\mathbf{J}[\mathbf{y}^{(k)}]$ should be recalculated with updated values of $\mathbf{y}^{(k)}$. Here, a frequency/time domain alternating scheme by FFT is introduced to evaluate the values of $\mathbf{d}[\mathbf{y}^{(k)}]$ and $\mathbf{J}[\mathbf{y}^{(k)}]$. $\mathbf{d}(\mathbf{y})$ and $\partial \mathbf{d}(\mathbf{y})/\partial \mathbf{y}$ are known to be the harmonic components of $D(t)$ and $\partial D(t)/\partial \mathbf{y}$ respectively. The time domain discrete values of $F(t)$, $\dot{F}(t)$, $x(t)$, $\dot{x}(t)$, $\ddot{x}(t)$ and $\ddot{\bar{x}}(t)$ over an integral period are first obtained by inverse FFT to $\{\mathbf{F}\}$ and $\{\mathbf{a}\}$. Then the time domain discrete values of $D(t)$, corresponding to $\mathbf{y} = \mathbf{y}^{(k)}$, are computed by equation (11). By forward FFT to these time domain discrete values of $D(t)$, the values of $\mathbf{d}[\mathbf{y}^{(k)}]$ are obtained. Similarly, the values of $\mathbf{J}[\mathbf{y}^{(k)}]$ are evaluated by forward FFT to the time domain discrete values of $\partial D(t)/\partial \mathbf{y}$ at $\mathbf{y} = \mathbf{y}^{(k)}$. $\partial D(t)/\partial \mathbf{y}$ can be derived analytically as follows

$$\partial D(t)/\partial y_1 = \partial D(t)/\partial b = -\dot{x} - x\dot{x}|z|^n[(n+1)\beta \operatorname{sgn}(\dot{x}) + n\gamma \operatorname{sgn}(z)]\, \partial \operatorname{sgn}(z)/\partial z$$
$$-nx\dot{x}|z|^{n-1}[\beta \operatorname{sgn}(\dot{x}) + \gamma \operatorname{sgn}(z)], \qquad z = F - bx - m\ddot{x}, \tag{15a}$$

$$\partial D(t)/\partial y_2 = \partial D(t)/\partial \alpha = -\dot{x}, \qquad \partial D(t)/\partial y_3 = \partial D(t)/\partial \beta = \dot{x} \operatorname{sgn}(\dot{x}) \operatorname{sgn}(z)|z|^n, \tag{15b, c}$$

$$\partial D(t)/\partial y_4 = \partial D(t)/\partial \gamma = \dot{x}|z|^n,$$

$$\partial D(t)/\partial y_5 = \partial D(t)/\partial n = \dot{x}[\beta \operatorname{sgn}(\dot{x}) \operatorname{sgn}(z) + \gamma]|z|^n \ln|z|, \tag{15d, e}$$

where the derivative of the signum function sgn (z) is equal to twice the Dirac delta function $\delta(z)$. $\delta(z)$ is a generalized function which does not have specific functional values in common sense, and hence intractable to numerical computation. A common treatment is to replace the signum function with a continuous function. In the present study, the signum function is approximated by

$$\operatorname{sgn}(z) \cong S(z) = \begin{Bmatrix} +1, & z > v \\ (2 - |z|/v)z/v, & -v \leqslant z \leqslant v \\ -1, & z < -v \end{Bmatrix}, \tag{16}$$

and its derivative

$$\frac{\partial \operatorname{sgn}(z)}{\partial z} \cong S'(z) = \begin{Bmatrix} 0, & z > v \\ (2/v)(1 - |z|/v), & -v \leqslant z \leqslant v \\ 0, & z < -v \end{Bmatrix}, \tag{17}$$

where the regularization parameter v is a small positive real number. The use of this function is due to two virtues: $S(z)$ is exactly equal to sgn (z) for $|x| > v$; $S'(z)$ is a continuous function like $S(z)$.

Usually, the periodic vibration tests are carried out under a wide range of frequencies and amplitudes. As a result, certain groups of the excitation and response signals $F_j(t)$, $x_j(t)$ $(j = 1, 2, \ldots, M)$ with different frequencies and amplitudes are measured and are used for parameter identification. In this situation, the objective function for least squares is

$$\min g(\mathbf{y}) = \sum_{j=1}^{M} w_j \|\mathbf{d}_j(\mathbf{y})\|^2 = \sum_{j=1}^{M} w_j \mathbf{d}_j^{\mathrm{T}} \mathbf{d}_j, \tag{18}$$

where w_j is a weight factor. Only the number of iterated equations is extended from $(2N + 1)$ to $(2N + 1)M$ and the solution process is similar.

3.2. NUMERICAL SIMULATION

A series of numerical simulations [26] have been performed to verify the validity of the proposed identification method. Four aspects have been addressed in these examples: (a) The applicability of the proposed method to various hysteretic systems including softening, hardening as well as quasi-linear systems; (b) The effect of different levels and types of the corrupted noise on the identification accuracy. The noise is simulated by the uniformly distributed random variables and by the normally distributed random variables; (c) Comparison of identification results from the observed signals with different frequencies. Albeit the hysteretic restoring force is rate-independent, the inertial force arising from different frequencies still affects the identification results; (d) Comparison of identification accuracy from the force controlled tests and from the displacement controlled tests.

Presented here is a special example with the aim of showing the nearly redundant parameter phenomenon. Emphasis is laid on observing the influence of noise level on the identification accuracy while the frequency effect is excluded by considering quasi-static excitations. Two sets of model parameters are considered, set 1 with $b = 0{\cdot}1$, $\alpha = 1{\cdot}0$, $\beta = 0{\cdot}5$, $\gamma = 0{\cdot}5$, $n = 1{\cdot}5$ and set 2 with identical values except $\beta = 0{\cdot}8$, $\gamma = 0{\cdot}2$. Both sets of the parameters correspond to softening hysteretic systems with the same extreme value $z_m = 1$. The output data of force controlled tests are simulated by calculating three groups of steady state displacement responses $x_j(t)$ $(j = 1, 2, 3)$ under force periodic exctitation $F_j(t) = F_j \cos t$ $(F_1 = 1{\cdot}0, F_2 = 2{\cdot}0, F_3 = 3{\cdot}0)$. Similarly, the resulting periodic forces $F_j(t)$ $(j = 1, 2, 3)$ corresponding to the prescribed displacement sequences $x_j(t) = A_j \cos t$ $(A_1 = 2{\cdot}0, A_2 = 4{\cdot}0, A_3 = 6{\cdot}0)$ are simulated as the output data of displacement controlled tests. The true hysteresis loops under these conditions are illustrated in Figure 1.

The force controlled and displacement controlled numerical experiments of the system with the parameters of set 1 are first performed. Only the output observation signals are contaminated with noise. The discrete noise corrupted output signals for the force controlled tests are obtained by

$$\bar{x}_j(t_i) = x_j(t_i) + \epsilon r_i X_j \tag{19}$$

TABLE 1

Identification results of set 1 *from force controlled tests*

Model parameters	Noise free	ϵ (using 1-period signals)			ϵ (using 8-period signals)		
		0·01	0·05	0·10	0·01	0·05	0·10
b	0·1000	0·1000	0·0993	0·0975	0·1000	0·0999	0·0998
α	1·0000	1·0237	1·0835	2·1310	0·9924	0·9618	0·9225
β	0·5000	0·3944	0·1960	0·1195	0·4956	0·4687	0·3936
γ	0·5000	0·6322	0·8928	2·0122	0·4975	0·4962	0·5341
n	1·5000	1·3736	0·7011	0·1477	1·4723	1·3508	1·2081

where r_i''s are a sequence of normally distributed random variables with zero mean and unit variance, X_j is the amplitude of $x_j(t)$ and the parameter ϵ represents the noise level. For the displacement controlled tests, the noise corrupted output data are given by

$$\bar{F}_j(t_i) = F_j(t_i) + \epsilon r_i F_j, \tag{20}$$

where F_j is the amplitude of $F_j(t)$.

Table 1 and Table 2 show the identification results of model parameters under various noise levels. No constraint or hypothesis on the model parameters is introduced in the estimate process. The weight w_j is taken as unity. Different lengths of discrete signals are used for identification. In the noise free case, the exact values of the parameters can be identified even using 1-period signals. The accuracy of identification is reduced with the increase of the level of corrupted noise. In the presence of serious noise, the identification results from 1-period signals may be very poor. However, increasing the length of signals used for identification would significantly improve the identification accuracy. Satisfactory identification results are obtained when using a certain number of periods of the signals. In actual experiments, usually the discrete time domain signals with enough length are recorded and are used for identification.

A comparison between Table 1 and Table 2 indicates that better identification results can be obtained from the displacement controlled tests than from the force

TABLE 2

Identification results of set 1 *from displacement controlled tests*

Model parameters	Noise free	ϵ (using 1-period signals)			ϵ (using 8-period signals)		
		0·01	0·05	0·10	0·01	0·05	0·10
b	0·1000	0·0999	0·0989	0·0966	0·1000	0·1002	0·1003
α	1·0000	0·9925	0·9717	0·9558	0·9987	0·9934	0·9871
β	0·5000	0·5148	0·5672	0·6180	0·5015	0·5074	0·5142
γ	0·5000	0·4743	0·3852	0·2969	0·4963	0·4817	0·4641
n	1·5000	1·5166	1·5215	1·4410	1·5010	1·5040	1·5060

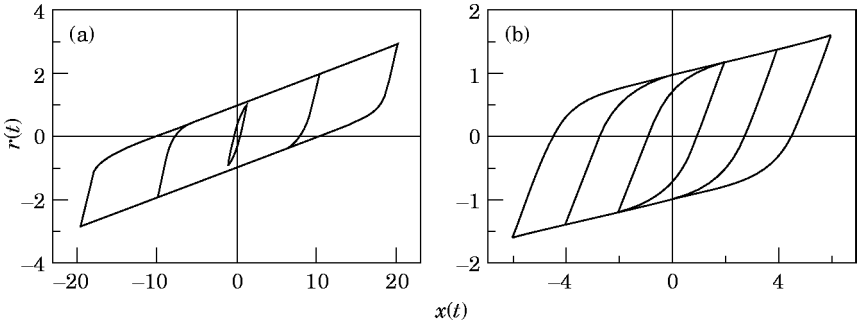

Figure 2. Identified hysteresis loops of set 1 from noise corrupted data ($\epsilon = 0{\cdot}10$): (a) force controlled tests; (b) displacement controlled tests.

controlled tests. Considering the rate-independent nature of the hysteretic restoring force, the displacement controlled cyclic loading tests can be readily executed using hydraulic actuators. Observation is now made on the identification results using 8-period signals. When the signals are noise corrupted corresponding to $\epsilon = 0{\cdot}10$, the identification results from the displacement controlled tests are only slightly different from the true values, and those from the force controlled tests, although possessing relatively large discrepancies, are still acceptable. Figure 2 depicts the theoretical hysteresis loops produced using the identified model parameters under $\epsilon = 0{\cdot}10$. They are excellently agreeable to the true hysteresis loops illustrated in Figure 1.

Numerical experiments are then implemented to the system with the parameters of set 2. The noise is now contaminated in a different manner. The discrete noise corrupted output data for the force controlled tests and for the displacement controlled tests are simulated respectively as

$$\bar{x}_j(t_i) = (1 + \epsilon r_i)x_j(t_i), \qquad \bar{F}_j(t_i) = (1 + \epsilon r_i)F_j(t_i), \tag{21, 22}$$

where r_i's are a sequence of random variables with uniform distribution within the interval $(-1, 1)$. The parameter ϵ represents the ratio of noise to signal.

Table 3 and Table 4 list the identification results of the model parameters under various noise levels and using different lengths of data. Exactly accurate values of the parameters are identified from noise free data. The observation signals with

TABLE 3

Identification results of set 2 from force controlled tests

Model parameters	Noise free	ϵ (using 1-period signals)			ϵ (using 8-period signals)		
		0·01	0·05	0·10	0·01	0·05	0·10
b	0·1000	0·1000	0·0998	0·0996	0·1000	0·1000	0·0999
α	1·0000	1·0141	1·1973	1·2889	1·0088	1·0588	1·1551
β	0·8000	0·7942	0·3764	0·1685	0·7914	0·7217	0·5718
γ	0·2000	0·2199	0·8208	1·1211	0·2175	0·3369	0·5829
n	1·5000	1·4579	1·1257	1·0386	1·4804	1·3654	1·1902

TABLE 4

Identification results of set 2 from displacement controlled tests

Model parameters	Noise free	ϵ (using 1-period signals)			ϵ (using 8-period signals)		
		0·01	0·05	0·10	0·01	0·05	0·10
b	0·1000	0·1001	0·1006	0·1011	0·1000	0·1002	0·1004
α	1·0000	0·9965	0·9832	0·9679	0·9989	0·9947	0·9896
β	0·8000	0·8106	0·8538	0·9093	0·8024	0·8121	0·8244
γ	0·2000	0·1855	0·1273	0·0544	0·1964	0·1819	0·1638
n	1·5000	1·5086	1·5415	1·5791	1·5028	1·5138	1·5269

enough length are most desirable to achieve satisfactory identification results. It appears again that the identification results from the displacement controlled tests are evidently better than those from the force controlled tests.

For the displacement controlled tests, so long as a certain number of periods of signals are used, satisfactory identification results are always obtained even the signals are seriously noise corrupted. For the force controlled tests, however, the estimated values of the parameters β and γ deviate gradually from the true values with the increase of noise level. It is interesting to note the identification results with $\epsilon = 0{\cdot}10$ close to set 1 rather than to set 2. They still yield the extreme value z_m equal almost to 1·0. Figure 3 shows the corresponding theoretical hysteresis loops generated using the identified model parameters under $\epsilon = 0{\cdot}10$. Although the identified values of the parameters β and γ are completely distinct from the true values, the identified hysteresis loops coincide well with the true loops. In this sense, such estimated values of the model parameters are still acceptable identification results.

As shown in Figure 1, the model parameters of set 1 and set 2 produce almost identical hysteresis loops. In fact different combinations of β and γ mainly affect the paths of inner branches (minor loops). The two cases exhibit almost the same responses for a wide range of cyclical loading amplitudes. A further comparison of the response harmonic components between the two cases shows that [26], under displacement loading the harmonic components of force response for set 1

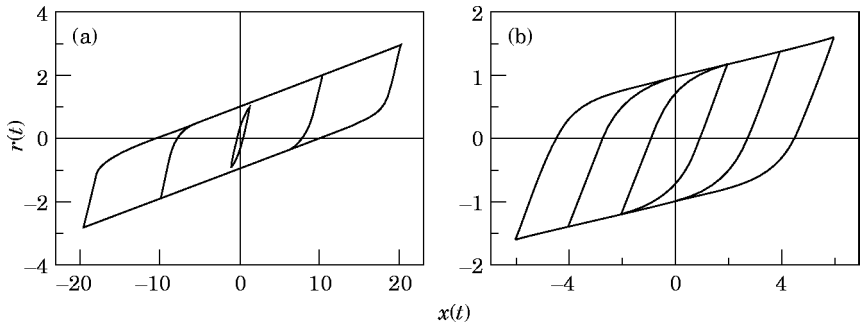

Figure 3. Identified hysteresis loops of set 2 from noise corrupted data ($\epsilon = 0{\cdot}10$): (a) force controlled tests; (b) displacement controlled tests.

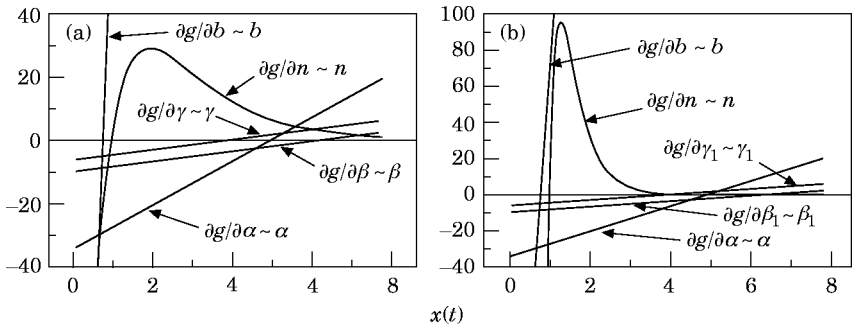

Figure 4. Sensitivity of objective function with respect to model parameters: (a) sensitivity curves of formula 1; (b) sensitivity curves of formula 2.

are slightly different from the corresponding values for set 2. Under force loading, however, the harmonic components of displacement response are almost same for the two cases. This explains why the identification results from force controlled tests are poorer than those from displacement controlled tests. It is also expected that the accuracy of parameter identification can be improved if the observation data embrace more information of intermediate minor loops through multi-harmonic excitation.

3.3. SENSITIVITY ANALYSIS

Sensitivity analysis of the objective function $g(\mathbf{y})$ with respect to the identified parameters $\{\mathbf{y}\}$ is helpful for determining initial guesses and understanding convergency performance of iteration. The sensitivity function can be derived from equation (18) as

$$\frac{\partial g(\mathbf{y})}{\partial \mathbf{y}} = 2 \sum_{j=1}^{M} w_j \mathbf{d}_j^{\mathrm{T}} \frac{\partial \mathbf{d}_j}{\partial \mathbf{y}}, \tag{23}$$

where $\mathbf{d}_j$ and $\partial \mathbf{d}_j / \partial \mathbf{y}$ are the function vector and Jacobian matrix. They can be readily evaluated by the frequency/time domain alternating algorithm.

The estimate scheme can be constructed with different objective function sensitivities. For instance, equation (1) can be transformed as the following expression

$$r(t) = bx(t) + \alpha z_1(t), \qquad \dot{z}_1(t) = \dot{x}(t) - \beta_1 |\dot{x}(t)| z_1(t) |z_1(t)|^{n-1} - \gamma_1 \dot{x}(t) |z_1(t)|^n \tag{24a, b}$$

by letting

$$z_1 = z/\alpha = \bar{z}/\bar{\alpha}, \qquad \beta_1 = \beta \alpha^{n-1} = \bar{\beta} \bar{\alpha}^{n-1}, \qquad \gamma_1 = \gamma \alpha^{n-1} = \bar{\gamma} \bar{\alpha}^{n-1}, \tag{25}$$

The model parameters relevant to equation (24) are also five, i.e., $\{\mathbf{y}\} = \{b \ \alpha \ \beta_1 \ \gamma_1 \ n\}^{\mathrm{T}}$. However, the objective function sensitivity of an estimate scheme based on equation (24) will be different. Figure 4 presents the objective function sensitivity curves of a softening system observed under noise

contamination. Here formula 1 refers to the estimate scheme based on equation (3) with the identified parameters $\{\mathbf{y}\} = \{b\ \alpha\ \beta\ \gamma\ n\}^{\mathrm{T}}$, while formula 2 is based on equation (24) with $\{\mathbf{y}\} = \{b\ \alpha\ \beta_1\ \gamma_1\ n\}^{\mathrm{T}}$. When evaluating the sensitivity with respect to a specific parameter, the other parameters are constantly fixed to their true values. It is seen in Figure 4, the sensitivity curves except that with respect to the parameter n are all monotone increasing functions. The sensitivity curve $\partial g/\partial n$ versus n is not monotonic, which first increases and then decreases to approach zero with the increase of n. An inappropriate initial guess of n may lead to convergence difficulty or incorrect solution. This also explains why most estimate methods do not include n as a parameter to be identified.

4. IMPLEMENTATION TO WIRE–CABLE ISOLATORS

A comprehensive experimental study on the static and dynamic hysteretic behavior of wire–cable isolators has been carried out [32]. Figure 5 shows the schematic of tested wire–cable isolators. A hanging shaking platform, as shown in Figure 6, has been developed for experiments on wire–cable isolators. In this setup, two rigid plates are hung in parallel upon a trestle, through nearly frictionless hinges connected with four rigid steel tubes, to form a double pendulum system. The isolator is mounted and fixed with its aluminum retainer bars to the upper and lower plates. The upper plate on the top of the isolator is fixed horizontally to the trestle through a force transducer (load cell) that measures the restoring force. The lower plate under the isolator is excited on one end, and connected on the other to an LVDT transducer to monitor isolator displacement. Excitation signals are supplied by a sine random generator which harmonically drives the lower plate. Besides the LVDT displacement transducer, an accelerometer is also mounted at the lower plate to measure acceleration and the signal is integrated digitally to obtain the displacement which can be used for comparison with the signal of the LVDT. The restoring force, displacement and acceleration are measured via charge amplifier, low pass filter and digitized through an A/D converter to a personal computer.

The hysteretic behavior of friction-type isolators is affected by static preloading. Hence the shaking platform is designed as a hanging double pendulum to eliminate vertical preloading owing to the upper plate weight. Also, the pendulum length is designed to be long enough relative to the motion of the isolators. Relative movement between the two plates can provide an almost pure shear deformation in the isolator. An advantage of this setup is that it allows direct

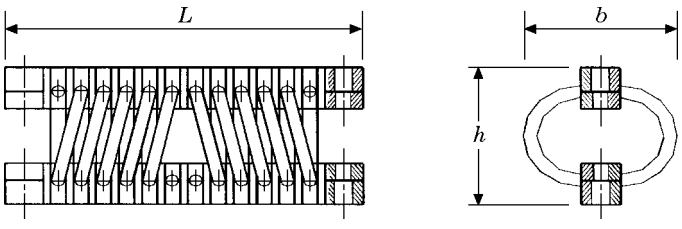

Figure 5. Schematic of tested wire–cable isolators.

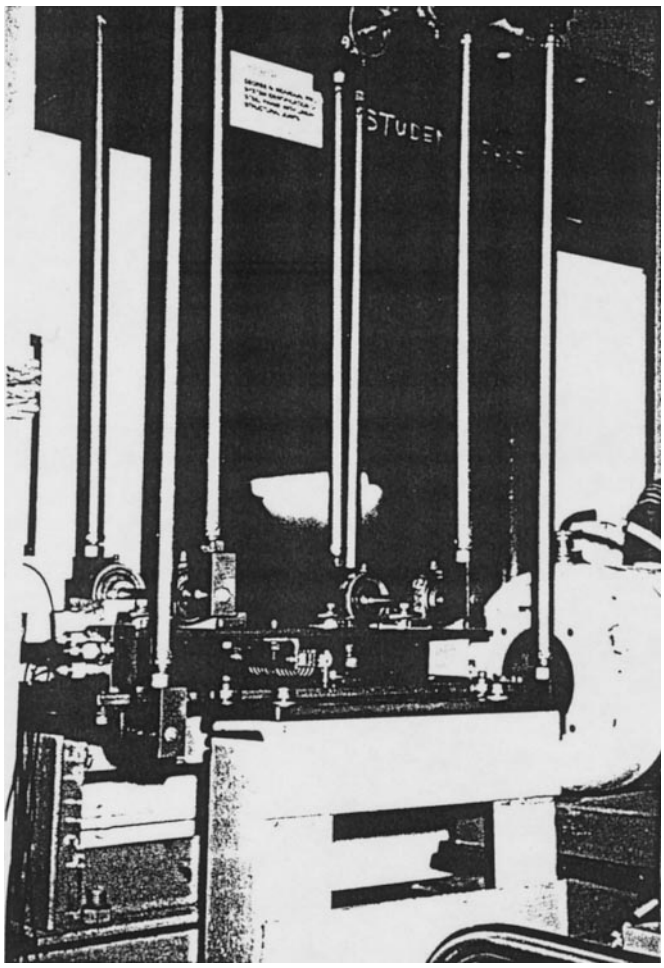

Figure 6. Setup of hanging shaking platform.

measurements of the restoring force (not exciting force) and response (displacement and acceleration) signals. The rate-independent nature of wire–cable isolators in the low frequency range has been experimentally verified as shown in Figure 7.

One of the wire–cable isolators, with length $L = 112$ mm, width $b = 40$ mm and height $h = 32$ mm, is tested in shear direction by imposing periodic sinusoidal motion of specified vibration amplitudes and frequencies. The displacement and restoring force periodic signals are generated for the frequency range 5–50 Hz, and for different amplitudes at each specific frequency. Figure 8 shows the measured hysteresis loops, after low pass filtering, with different vibration amplitudes at the frequency $f = 5$ Hz and $f = 10$ Hz respectively. The displacement and restoring force signals are recorded simultaneously and are sampled synchronously by using a high speed data acquisition processor. Non-synchronism of the displacement and restoring force signals during recording and sampling will seriously distort the shape and area of hysteresis loops.

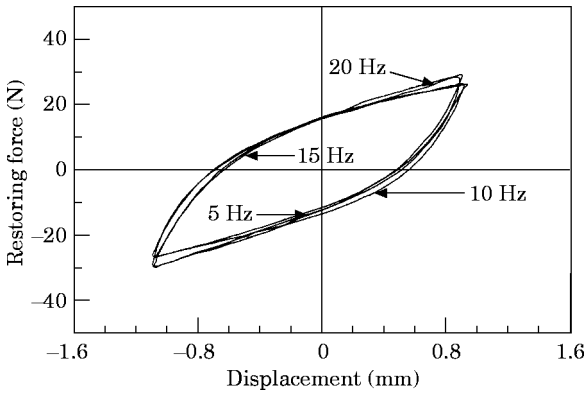

Figure 7. Experimental hysteresis loops with different frequencies.

A total of 20 groups of recorded displacement and restoring force signals with different frequencies and amplitudes are used for identification, i.e., $M = 20$. The order number of harmonics truncated is taken as $N = 5$. The parameter identification is performed by taking the weight factor w_j equal to 1, $A_j^{-1/2}$ and A_j^{-1} respectively, where A_j is the amplitude of the jth displacement signal $x_j(t)$. Four sets of initial guesses,

$$\{\mathbf{y}^{(0)}\} = \{0{\cdot}1\ \ 0{\cdot}1\ \ 0{\cdot}1\ \ 0{\cdot}1\ \ 1{\cdot}0\}^{\mathrm{T}}, \qquad \{\mathbf{y}^{(0)}\} = \{1{\cdot}0\ \ 1{\cdot}0\ \ 1{\cdot}0\ \ 1{\cdot}0\ \ 1{\cdot}0\}^{\mathrm{T}},$$

$$\{\mathbf{y}^{(0)}\} = \{5{\cdot}0\ \ 5{\cdot}0\ \ 5{\cdot}0\ \ 5{\cdot}0\ \ 1{\cdot}0\}^{\mathrm{T}}, \qquad \{\mathbf{y}^{(0)}\} = \{10{\cdot}0\ \ 10{\cdot}0\ \ 10{\cdot}0\ \ 10{\cdot}0\ \ 1{\cdot}0\}^{\mathrm{T}}$$

are tried to carry out the iterative solution using formula 1 and to check the uniqueness of convergency. The convergency takes place for all these initial guesses. With a specific weight factor, the iteration starting from different initial guesses approaches the same set of converged values. Table 5 lists the identification results. The parameter estimation is also performed using formula 2 and identical values are obtained.

By using the identified values of the model parameters, the Bouc–Wen model generates the theoretical hysteresis loops as shown in Figure 9. It is seen that the Bouc–Wen model with the identified parameters provides a good representation of the measured hysteresis loops. Though the values of the model parameters

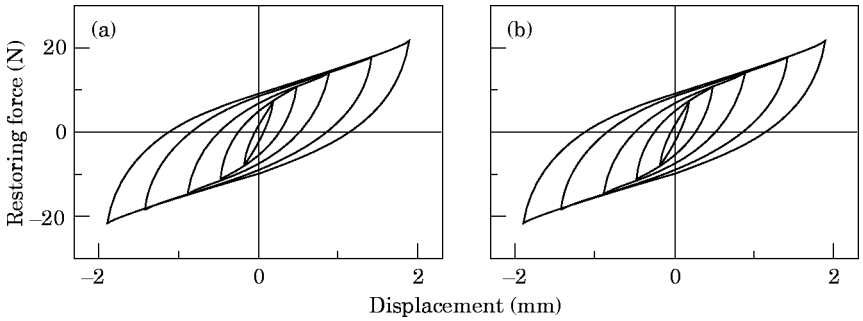

Figure 8. Measured hysteresis loops with different amplitudes after low pass filtering: (a) hysteresis loops at $f = 5$ Hz; (b) hysteresis loops at $f = 10$ Hz.

TABLE 5

Identification results of a wire–cable isolator

Model parameters	$w_j = 1$	$w_j = A_j^{-1/2}$	$w_j = A_j^{-1}$
b	6·078	6·674	7·423
α	34·422	38·017	40·334
β	8·940	8·780	8·207
γ	1·500	1·423	0·503
n	0·525	0·594	0·710

obtained by using different weight factors are different, the resulting hysteresis loops appear similar. It has been shown [25] that a slight variation of the model parameter n will require a significant change in other parameters in order to fit the same hysteresis loops. The exponential parameter n governs the transition smoothness of the hysteresis loops. If n is invariant, the identified model parameters by using different weight factors will be more consistent.

Since the isolator, when under test, vibrates with nearly single harmonic motion, the theoretical hysteresis loops are produced under the displacement loading $x(t) = A_j \cos t$. It has been shown [23, 25] that the hysteresis loop characteristics of an isolator under sinusoidal motion are completely described by the harmonic components of its restoring force. The restoring force harmonic components of the Bouc–Wen hysteretic system subjected to a periodic displacement loading can be readily evaluated by means of a steady state response analysis [24]. Therefore,

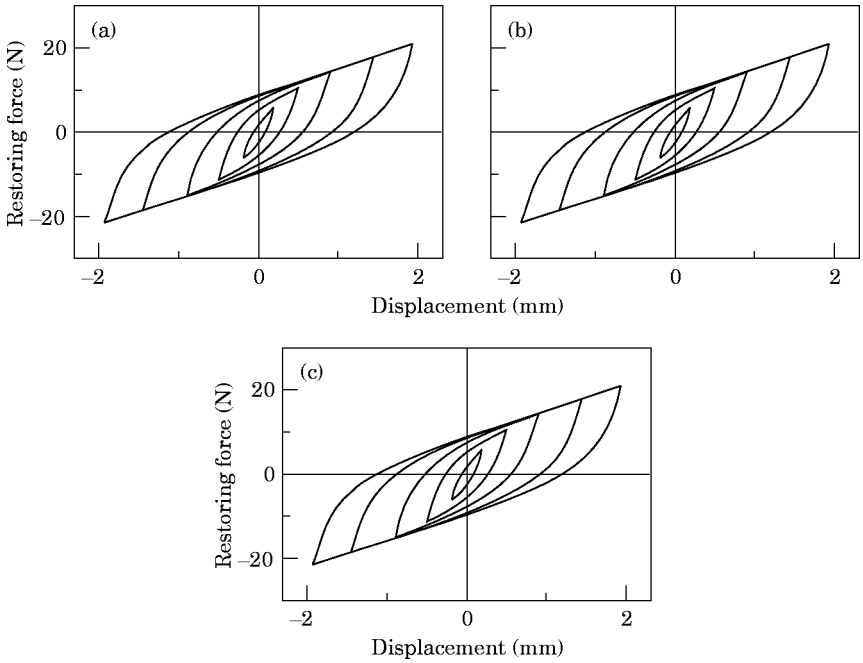

Figure 9. Theoretical hysteresis loops produced by identified model parameters: (a) weight factor $w_j = 1$; (b) weight factor $w_j = A_j^{-1/2}$; (c) weight factor $w_j = A_j^{-1}$.

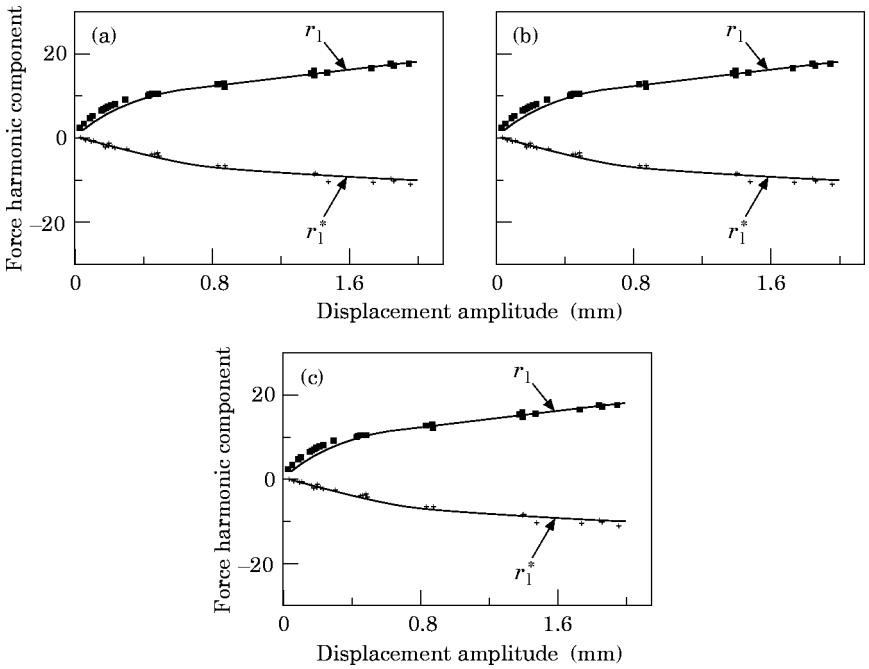

Figure 10. First order harmonic components of restoring force: (a) weight factor $w_j = 1$; (b) weight factor $w_j = A_j^{-1/2}$; (c) weight factor $w_j = A_j^{-1}$. Key: —, identified; ■, +, measured.

a comparison between the measured and identified harmonic components will verify the accuracy of parameter identification.

Figure 10 illustrates such a comparison, in which the solid lines indicate the calculated (identified) first order harmonic components of the restoring force of the identified model subjected to displacement loading $x(t) = A \cos t$, while the scattered points denote the measured values. It is observed that when $w_j = 1$, because those of the measured displacement force signals with large amplitudes play a predominant role in identification, some discrepancy between the measured and identified harmonic components is present in the small amplitude range. When $w_j = A_j^{-1}$, the discrepancy in the small amplitude range is eliminated but the error in the large amplitude range increases relatively. In the case of $w_j = A_j^{-1/2}$, a compromise situation is achieved. Apparently, the identification accuracy can be ameliorated by introducing proper weight factors.

5. CONCLUSIONS

An identification method has been proposed to estimate the model parameters of the Bouc–Wen hysteretic systems from periodic vibration tests. Applying the harmonic balance technique leads to a frequency domain least squares estimate with appropriate cost function. The LM iteration algorithm is formulated for the parameter estimation, in which a frequency/time domain alternating scheme by FFT is introduced to perform the numerical calculation concerned. The conventional time domain estimate methods [12, 16] used to solve the same

problem require a numerical solution of about 20 simultaneous non-linear differential equations at each iterative step, hence involving a great amount of computational effort. The frequency/time domain alternating scheme present here is computationally efficient.

Numerical simulations show that the proposed frequency domain method is insensitive to the corrupted noise. Usually, when the signal-to-noise ratio is greater than twenty ($\epsilon \leqslant 0{\cdot}05$) and the experimental data used for identification are long enough, all the model parameters can be estimated reliably. When the signal is contaminated with serious noise, some of the identified parameters may deviate from their true values. However, the theoretical hysteresis loops produced using such estimated values still coincide well with the true loops. In this sense, the identification results are considered to be reasonable. With the same level of noise, the identification results from displacement controlled experiments are more accurate than those from force controlled experiments.

The proposed method has been applied to the modelling and identification of the experimental hysteretic behavior of a wire–cable isolator. A good representation of the measured hysteresis loops is obtained from the identification results. The case study shows that the identification accuracy is ameliorated by introducing proper weight factors. The weight factors can be taken to be inversely proportional to the amplitudes (or their roots) of measured displacement or force periodic signals.

ACKNOWLEDGMENTS

This study is supported in part by the Research Grants Committee (RGC) of Hong Kong Government and partly by the Hong Kong Polytechnic University. These supports are gratefully acknowledged.

REFERENCES

1. M. A. Cutchins, J. E. Cochran, S. Guest, N. G. Fitz-Coy and M. L. Tinker 1987 *The Role of Damping in Vibration and Noise Control ASME* DE-**5**, 197–204. An investigation of the damping phenomena in wire rope isolators.
2. S. Nagarajaiah, A. M. Reinhorn and M. C. Constantinou 1991 *ASCE Journal of Structural Engineering* **117**, 2035–2054. Nonlinear dynamic analysis of 3-D-base-isolated structures.
3. R. S. Jangid and T. K. Datta 1994 *ASCE Journal of Structural Engineering* **120**, 1–22. Nonlinear response of torsionally coupled base isolated structure.
4. J. Prendergast 1995 *ASCE Civil Engineering* **65**, 58–61. Seismic isolation in bridges.
5. P. Dupont, P. Kasturi and A. Stokes 1997 *Journal of Sound and Vibration* **202**, 203–218. Semi-active control of friction dampers.
6. R. Bouc 1971 *Acustica* **24**, 16–25. Modèle mathématique d'hystérésis.
7. Y. K. Wen 1976 *ASCE Journal of the Engineering Mechanics Division* **102**, 249–263. Method of random vibration of hysteretic systems.
8. M. C. Constantinou and I. G. Tadjbakhsh 1985 *ASCE Journal of Structural Engineering* **111**, 705–721. Hysteretic dampers in base isolation: random approach.

9. H. R. Lo, J. K. Hammond and M. G. Sainsbury 1988 *Proceedings of the 6th International Modal Analysis Conference*, *Florida*, **II**, 1453–1459. Nonlinear system identification and modelling with application to an isolator with hysteresis.
10. M. Constantinou, A. Mokha and A. Reinhorn 1990 *ASCE Journal of Structural Engineering* **116**, 455–474. Teflon bearings in base isolation, II: modeling.
11. G. F. Demetriades, M. C. Constantinou and A. M. Reinhorn 1993 *Engineering Structures* **15**, 321–334. Study of wire rope systems for seismic protection of equipment in buildings.
12. M. Yar and J. K. Hammond 1987 *Journal of Sound and Vibration* **117**, 161–172. Parameter estimation for hysteretic systems.
13. R. H. Sues, S. T. Mau and Y. K. Wen 1988 *ASCE Journal of Engineering Mechanics* **114**, 833–846. Systems identification of degrading hysteretic restoring forces.
14. M. Hoshiya and O. Maruyama 1987 *Stochastic Approaches in Earthquake Engineering*: *Lecture Notes in Engineering* **32**, 68–86. Kalman filtering of versatile restoring systems.
15. J.-S. Lin and Y. Zhang 1994 *Computers and Structures* **52**, 757–764. Nonlinear structural identification using extended Kalman filter.
16. J. B. Roberts and A. H. Sadeghi 1990 *Structural Safety* **8**, 45–68. Sequential parametric identification and response of hysteretic oscillators with random excitation.
17. A. G. Chassiakos, S. F. Masri, A. Smyth and J. C. Anderson 1995 *Proceedings of the American Control Conference*, *Seattle*, **III**, 2349–2353. Adaptive methods for identification of hysteretic structures.
18. S. Bellizzi and R. Bouc 1988 *Nonlinear Stochastic Dynamic Engineering Systems*: *Proceedings of IUTAM Symposium*, 467–476. Identification of the hysteresis parameters of a nonlinear vehicle suspension under random excitation.
19. C.-H. Loh and S.-T. Chung 1993 *Earthquake Engineering and Structural Dynamics* **22**, 129–150. A three-stage identification approach for hysteretic systems.
20. H. Lekuch 1986 *Noise and Vibration Control Worldwide* **17**, 240–245. Shock and vibration isolation in severe environments.
21. M. L. Tinker and M. A. Cutchins 1992 *Journal of Sound and Vibration* **157**, 7–18. Damping phenomena in a wire rope vibration isolation system.
22. M. L. Tinker and M. A. Cutchins 1994 *Journal of Sound and Vibration* **176**, 415–428. Instabilities in a non-linear model of a passive damper.
23. J. M. Ko, Y. Q. Ni and Q. L. Tian 1992 *The International Journal of Analytical and Experimental Modal Analysis* **7**, 111–127. Hysteretic behavior and empirical modeling of a wire–cable vibration isolator.
24. C. W. Wong, Y. Q. Ni and S. L. Lau 1994 *ASCE Journal of Engineering Mechanics* **120**, 2271–2298. Steady-state oscillation of hysteretic differential model, I: response analysis.
25. C. W. Wong, Y. Q. Ni and J. M. Ko 1994 *ASCE Journal of Engineering Mechanics* **120**, 2299–2325. Steady-state oscillation of hysteretic differential model, II: performance analysis.
26. Y. Q. Ni 1997 *Ph.D. Dissertation*, *The Hong Kong Polytechnic University*, *Hong Kong*. Dynamic response and system identification of nonlinear hysteretic systems.
27. A. Visintin 1994 *Differential Models of Hysteresis*. Berlin: Springer-Verlag.
28. H. Ozdemir 1976 *Ph.D. Dissertation*, *University of California*, *Berkeley*. Nonlinear transient dynamic analysis of yielding structures.
29. M. A. Bhatti and K. S. Pister 1981 *Earthquake Engineering and Structural Dynamics* **9**, 557–572. A dual criteria approach for optimal design of earthquake-resistant structural systems.
30. T. Fujita, Y. Sasaki, S. Fujimoto and C. Tsuruya 1990 *JSME International Journal*: *Series III* **33**, 427–434. Seismic isolation of industrial facilities using lead-rubber bearing.

31. C.-Y. PENG and W. D. IWAN 1992 *Earthquake Engineering and Structural Dynamics* **21**, 695–712. An identification methodology for a class of hysteretic structures.
32. C. W. WONG, S. ZHAN and J. M. KO 1995 *Proceedings of the International Conference on Structural Dynamics*, *Vibration*, *Noise and Control*, *Hong Kong*, **II**, 1148–1153. Experimental study on wire–cable isolator.